



THE UNIVERSITY *of* EDINBURGH

Edinburgh Research Explorer

The kinematics of Galactic disc white dwarfs in Gaia DR2

Citation for published version:

Rowell, N & Kilic, M 2019, 'The kinematics of Galactic disc white dwarfs in Gaia DR2', *Monthly Notices of the Royal Astronomical Society*. <https://doi.org/10.1093/mnras/stz184>

Digital Object Identifier (DOI):

[10.1093/mnras/stz184](https://doi.org/10.1093/mnras/stz184)

Link:

[Link to publication record in Edinburgh Research Explorer](#)

Document Version:

Peer reviewed version

Published In:

Monthly Notices of the Royal Astronomical Society

General rights

Copyright for the publications made accessible via the Edinburgh Research Explorer is retained by the author(s) and / or other copyright owners and it is a condition of accessing these publications that users recognise and abide by the legal requirements associated with these rights.

Take down policy

The University of Edinburgh has made every reasonable effort to ensure that Edinburgh Research Explorer content complies with UK legislation. If you believe that the public display of this file breaches copyright please contact openaccess@ed.ac.uk providing details, and we will remove access to the work immediately and investigate your claim.



The kinematics of Galactic disc white dwarfs in Gaia DR2

Nicholas Rowell,¹★ Mukremin Kilic²

¹*Institute for Astronomy, University of Edinburgh, Royal Observatory, Blackford Hill, Edinburgh EH9 3HJ, UK*

²*Homer L. Dodge Department of Physics and Astronomy, University of Oklahoma, 440 W. Brooks St., Norman, OK, 73019, USA*

Accepted XXX. Received YYY; in original form ZZZ

ABSTRACT

We present an analysis of the kinematics of Galactic disc white dwarf stars in the Solar neighbourhood using data from Gaia Data Release 2. Selection of white dwarfs based on parallax provides the first large, kinematically unbiased sample of Solar neighbourhood white dwarfs to date. Various classical properties of the Solar neighbourhood kinematics have been detected for the first time in the WD population.

The disc white dwarf population exhibits a correlation between absolute magnitude and mean age, which we exploit to obtain an independent estimate of the Solar motion with respect to the Local Standard of Rest. This is found to be $(U, V, W)_{\odot} = (9.5 \pm 1.2, 7.5 \pm 1.2, 8.2 \pm 1.2)$ kms⁻¹. The UW components agree with studies based on main sequence stars, however the V component differs and may be affected by systematics arising from metallicity gradients in the disc. The velocity ellipsoid is shown to vary strongly with magnitude, and exhibits a significant vertex deviation in the UV plane of around 15 degrees, due to the non-axisymmetric Galactic potential.

The results of this study provide an important input to proper motion surveys for white dwarfs, which require knowledge of the velocity distribution in order to correct for missing low velocity stars that are culled from the sample to reduce subdwarf contamination.

Key words: (stars:) white dwarfs – Galaxy: disc – Galaxy: kinematics and dynamics – (Galaxy:) solar neighbourhood

1 INTRODUCTION

The stars in the vicinity of the Sun move under the combined gravitational influence of all the other stars, gas and dark matter in the Galaxy, and by analyzing their motions it is possible to infer aspects of the dynamical structure, evolution and physical processes at work in the Milky Way as a whole. These include the kinematic heating of stars through both secular processes and merger events, the local circular velocity and slope of the rotation curve, and the shape of the gravitational potential. Knowledge of the velocity distribution of stars is also relevant from a survey astronomy point of view, as it is a vital input when quantifying the completeness of proper motion surveys (e.g. Rowell & Hambly 2011, hereafter RH11; Lam et al. 2019).

This field has a long history, but went through something of a renaissance with the release of data from the Hipparcos mission (e.g. Feast & Whitelock 1997; Dehnen & Binney 1998; Mignard 2000; van Leeuwen 2007; Schönrich et al. 2010) which provided stringent constraints on various parameters of the Milky Way derived for the first time from absolute parallaxes. In particular, Dehnen & Binney (1998) (hereafter DB98) used a sample of 16054 main sequence (MS) stars to measure the Solar motion with respect to the local standard of rest (LSR), an important quantity for transforming

heliocentric velocities to a Galactic frame. This classic technique exploits the correlation between colour and mean age that exists for MS stars bluewards of the turn off of the old disk at $B - V \sim 0.6$; the break in the trend of velocity dispersion against colour that exists at this point is known as Parenago’s discontinuity. However, as explained by Schönrich et al. (2010) the DB98 methodology is undermined by metallicity gradients within the disc that lead to complex kinematic substructure in the colour–magnitude plane. This field is now set to be truly revolutionized by the data from the Gaia mission (Gaia Collaboration et al. 2016), the successor to Hipparcos, which ultimately aims to measure absolute parallaxes and proper motions at the microarcsecond level for more than one billion stars in the Milky Way down to $G \approx 20$. The second data release (DR2 – see Gaia Collaboration et al. 2018a) was published on 25th April 2018, and already contains over 1.3 billion sources with parallax accuracies of the order 700 μ as at the $G = 20$ faint end. Much progress is still to be made at reducing systematic errors by improving various instrument calibrations, but early studies demonstrate the enormous potential of the Gaia data. These include Bovy (2017), who measured the Oort Constants that parameterise the local stellar streaming velocity, obtaining the first significant estimates of the C and K terms. Gaia Collaboration et al. (2018b) used a subsample of 6.4 million FGK stars with full 6D phase space coordinates to draw 3D maps of the stellar velocity distribution with unprecedented accuracy, revealing rich substructure and complex streaming motions

★ E-mail: nr@roe.ac.uk (NR)

in the Galactic disk. On a larger scale, [Kawata et al. \(2019\)](#) used a sample of 218 Cepheids with Gaia proper motions to estimate several parameters of the Galactic rotation, including the centrifugal velocity, the slope of the circular speed curve, the local velocity dispersion and the Sun's peculiar velocity.

One avenue that has recently been opened by the Gaia DR2 is the possibility of conducting a kinematic study using the white dwarf (WD) stars in the Solar neighbourhood. Both Hipparcos and Gaia DR1 (TGAS) contain only very small numbers of WDs that cannot be used for a systematic study. Instead, the largest quantifiably-complete catalogues of WDs to date have been derived using the Reduced Proper Motion (RPM) method applied to ground based survey data. These include the Sloan Digital Sky Survey ([Kilic et al. 2006; Munn et al. 2017](#)), the SuperCOSMOS Sky Survey (RH11) and PanSTARRS 1 ([Lam et al. 2019](#)), each of which contain of order ~ 10000 WDs. The problem with these catalogues, from a kinematic point of view, is that the RPM method necessitates the use of a low tangential velocity threshold of around 30kms^{-1} , below which stars are rejected in order to limit contamination from subdwarfs. This results in a catalogue that is suitable for luminosity function studies but is inherently kinematically biased. Note that the SDSS spectroscopic WD catalogue ([Kleinman et al. 2013; Kepler et al. 2015](#)), which contains around 30000 WDs in total, is biased by the complex selection function for fibre allocation.

The Gaia DR2 on the other hand contains several hundred thousand WDs ([Gentile Fusillo et al. 2018](#)) that can be reliably identified based on parallax. The need to construct a robust sample within well characterized survey limits requires use of stricter selection criteria that reduces the useful sample size, but even so this is orders of magnitude larger than any previous comparable WD survey. Although in any magnitude-limited survey, such as that conducted by Gaia, WDs will exist in much smaller numbers than main sequence stars, analysis of their kinematics is still of importance for the following reasons:

- In a volume-limited sample such as the Solar neighbourhood the WDs make up a much more significant fraction of the population, and any study that omits them can only be an incomplete picture.
- The location of a WD in colour-magnitude space is independent of the progenitor star metallicity, which may avoid certain systematics that arise in similar studies that use MS stars, as described in [Schönrich et al. \(2010\)](#); briefly, metal-rich stars generally formed at $R < R_0$ and visit the Solar neighbourhood close to the apocentre of their orbit where their azimuthal velocities lag behind the local circular speed. As metallicity displaces the MS, this introduces substructure in the colour-magnitude diagram that correlates with kinematics.
- For Solar neighbourhood WDs there exists a correlation between absolute magnitude and mean age, analogous to the colour/age correlation that exists for MS stars, which can be exploited to obtain an independent determination of the motion of the Sun with respect to the local standard of rest.

The final point holds for any WD population that did not form in a single burst, and is due mainly to the monotonic cooling law ([Mestel 1952](#)). This magnitude/age correlation exists for essentially all realistic star formation histories, though the strength of the correlation varies and requires detailed modelling to quantify. In figure 1 (reproduced from [Rowell \(2013\)](#)) we depict the mean total stellar age as a function of bolometric magnitude for a range of simulated white dwarf populations of different star formation history. The correlation is strongest in the $M_{\text{bol}} = 13$ to 15 range and for the less burst-like star formation histories. The Gaia G magnitude is ex-

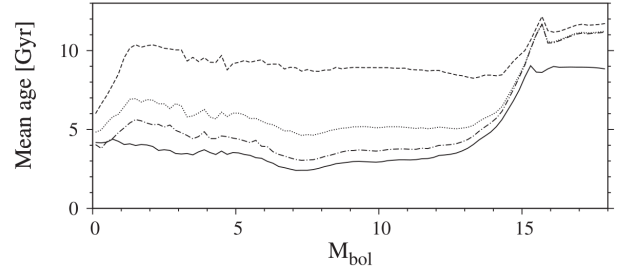


Figure 1. The mean total stellar age as a function of bolometric magnitude for a range of simulated white dwarf populations of different star formation rate $\psi(t)$. The solid and dot-dashed lines are for a constant ψ with a total age $T_0 = 10$ and 13 Gyr respectively; the dashed line is for $\psi(t) \propto \exp(-t/\tau)$ with $\tau = 3$ Gyr and $T_0 = 13$ Gyr; the dotted line is for $\psi(t) \propto (1 + \exp((t - t')/\tau)) - 1$ with $t' = 10$ Gyr, $\tau = 3$ Gyr and $T_0 = 13$ Gyr. This figure is reproduced from [Rowell \(2013\)](#).

pected to show a similar trend due to the extremely broad wavelength range leading to small bolometric corrections of $\Delta M_{\text{bol}} \leq 0.09$ for both H and He atmosphere WDs over the $G = 13$ to 15 range (P. Bergeron, priv. communication).

In this study we use Gaia DR2 to assemble a catalogue of 78,511 WDs in the solar neighbourhood. This is the largest kinematically complete sample of WDs to date. We use this to investigate several classical features of the Solar neighbourhood kinematics, including the asymmetric drift, local standard of rest and age-velocity dispersion relation. Note that this study is independent of WD cooling models, being based on only direct observational quantities. In section 2 we outline the construction of our WD sample. Section 3 explains the methods used to determine the kinematics, which are based on the proper motion deprojection method presented in DB98. We present our results in section 4 with further discussion in section 5, and draw conclusions in section 6.

2 WHITE DWARF SELECTION

The sample of white dwarfs (WDs) used in this work was obtained from the Gaia data by selection in the Hertzsprung-Russell diagram (HRD). We applied initial filters on the signal-to-noise of the photometry and astrometry to reject objects with relative parallax errors greater than 20% and errors on G_{BP}/G_{RP} flux greater than 10%. This reduces the scatter in the HRD and allows the absolute magnitude to be determined based on simple inversion of the parallax. We also place cuts on the *flux excess factor* to eliminate objects whose photometry is compromised by blending issues, and we reject objects further than 250pc from the Sun for reasons explained in section 3. This resulted in an initial sample of 3061480 objects drawn from the Gaia archive; the ADQL query that performs this selection is presented in appendix A.

We applied additional astrometric quality criteria to reduce contamination from objects with poor astrometric solutions, by rejecting objects with a Renormalised Unit Weight Error (RUWE; described in [Lindgren \(2018\)](#)) greater than 1.4. This has the effect of removing objects lying between the main sequence and white dwarf locus, which includes many partially resolved close pairs that the Gaia astrometric solution is not yet capable of handling properly. We also reject objects with tangential velocity greater than 150kms^{-1} as these are likely not disk members. This reduces the initial sample to 2644657 well-measured Solar neighbourhood disk

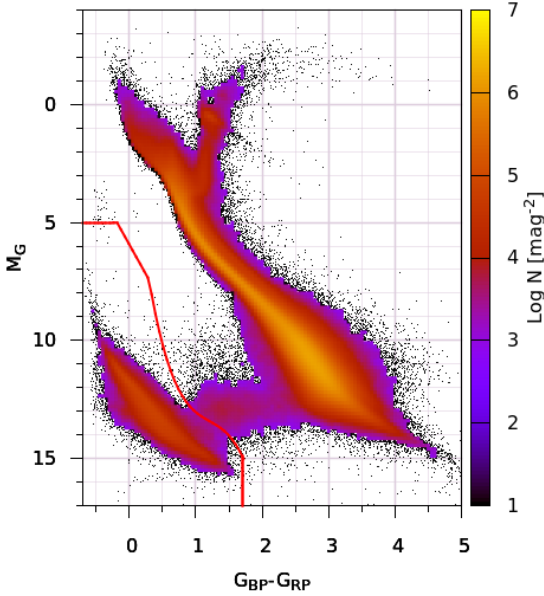


Figure 2. Hertzsprung-Russell diagram of 2644657 well-measured disk stars within 250 pc. The red line marks the WD selection region in the Gaia bands defined by [Gentile Fusillo et al. \(2018\)](#), which contains 79225 WDs. Sources have been filtered using the Renormalised Unit Weight Error (see text).

stars. The Hertzsprung-Russell diagram (HRD) of these objects is presented in figure 2.

We select WDs from the lower left region of the $M_G/G_{BP} - G_{RP}$ plane using the same criteria as [Gentile Fusillo et al. \(2018\)](#). This region is marked by a red boundary in figure 2, and contains 79225 WDs. There is also clearly a small amount of contamination from unresolved WD+dM systems lying in the region between the MS and WDs, which will add some degree of noise to our results in the M_G range ≈ 13 –15. Although the astrometry for these objects is presumably reliable, having passed our selection criteria, the photometry will be compromised. The fraction of contaminating sources as a function of M_G can be estimated from the red tail of the colour distribution; we estimate that the contamination is limited to less than a few percent at all magnitudes. We do not expect this level of contamination to have a significant effect on our results. We also restrict the analysis to WDs with absolute magnitudes in the range $[10:15.5]$ for the following reasons. Brighter than $M_G = 10$ there are very few WDs and the correlation with age is nonexistent. Fainter than $M_G = 15.5$, the WD population starts to become heavily contaminated by thick disk and spheroid objects that have different kinematics, as well as low and high mass WDs that have not followed the same evolutionary path as the rest of the population and so don't obey the same magnitude / mean age correlation. This results in a clean sample of 78511 WDs. The sky distribution of these is presented in figure 3. Note that the lower density of stars towards the Galactic centre is not due to dust extinction, as our sample is relatively local. Instead this is most likely caused by various issues that Gaia faces in crowded regions, in particular blending

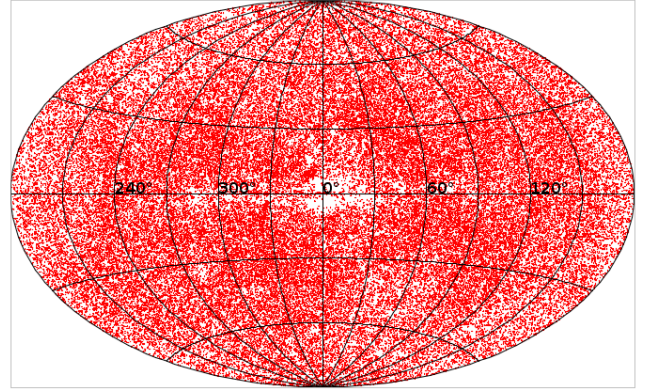


Figure 3. Sky distribution in Galactic coordinates of the 78511 WDs that pass our selection criteria. The lower density of sources towards the Galactic centre is most likely due to problems that Gaia faces in crowded regions, as explained in the text.

of objects in both the photometric and astrometric instruments, but also challenging cross-match and loss of faint stars due to onboard resource limitations.

3 METHODS

The WDs in Gaia DR2 have parallax and proper motion estimates but no radial velocities. Even the final Gaia catalogue will have few radial velocities for WDs, due to their intrinsic faintness and the fact Gaia's radial velocity spectrograph is tuned to the calcium triplet that does not appear in the spectra of the majority of WDs. Although the lack of radial velocities means the 3D space motion of individual stars cannot be recovered, we can still calculate the moments of the 3D velocity distribution by means of the proper motion deprojection technique introduced by DB98. In this method, we first correct the proper motions of stars for the effects of Galactic rotation using equation 1 from DB98, with values of the Oort constants $A = 15.3$ and $B = -11.9$ taken from [Bovy \(2017\)](#). The remaining tangential velocity of each star \underline{p} , which is estimated from the parallax and corrected proper motion, is related to the 3D space motion \underline{v} according to

$$\underline{p} = A \underline{v} \quad (1)$$

where the projection matrix A is defined by $\mathbb{I} - \hat{\underline{r}} \otimes \hat{\underline{r}}$, with $\hat{\underline{r}}$ the unit vector towards the star and \otimes denotes the outer product. Obviously, this equation cannot be inverted to obtain \underline{v} and as such the matrix A is singular. However, by averaging over a large number of stars distributed widely across the whole sky, the mean matrix $\langle A \rangle$ is non-singular and the equation can be inverted to obtain the mean velocity $\langle \underline{v} \rangle$ of the population relative to the Sun. The residual velocities of stars can be used to estimate the scalar velocity dispersion, and an extension of this method allows the full velocity dispersion tensor to be computed. We refer the reader to DB98 for further details. As explained in [McMillan & Binney \(2009\)](#), the method is strictly only applicable when the lines of sight to individual stars are uncorrelated with the stars' velocities. This criteria holds for stars within a limited distance from the Sun, beyond which the velocity dispersion varies with both radius and distance from the plane. For this reason we restrict the analysis to stars within 250pc. In any case, the Gaia apparent magnitude limit of $G \approx 21$ means that fainter than around $M_G \approx 13.7$ all our stars are within 250pc anyway, and according to

Rowell (2013) the correlation between magnitude and total age is very weak brighter than $M_G \approx 13$.

Note that this method is superior to simply assuming zero radial velocity and computing the sample mean and covariance, which is done in some studies. The assumption of zero radial velocity causes the mean velocity to be underestimated by (on average) one third. The velocity dispersion is also underestimated by up to one third due to a combination of the loss of the peculiar velocity along the line of sight and the bias in the estimated mean.

We apply the kinematic analysis independently to bins of different G magnitude. We tried bins containing equal numbers of stars, but this conceals important structure around the faint end of the range where there are relatively few stars. After some tests we settled on bins of a fixed width of $\Delta M_G = 0.125$.

4 RESULTS

We applied the methods described in section 3 to our sample of 78,511 WDs, independently on 44 bins of $\Delta M_G = 0.125$ between $M_G = 10$ and $M_G = 15.5$. Table 4 presents the mean velocity and velocity dispersion tensor for each magnitude bin. In this section we highlight some selected results from these data.

4.1 Mean velocity and the asymmetric drift

In figure 4 we plot the U , V , W components of the mean Solar motion with respect to the WDs, along with the quantity S from DB98 that is a scalar measure of the velocity dispersion. The most obvious feature is the rise in the V component towards faint magnitudes, which is a manifestation of the asymmetric drift. This is accompanied by a corresponding rise in the velocity dispersion as some of the original circular motion is scattered randomly into the U , W components. At magnitudes brighter than $M_G \approx 13$ there is no trend in V or S ; in this range the correlation between magnitude and mean age is nonexistent. No break analogous to Paranege's discontinuity is present; there is no equivalent of the MS turnoff colour in the WD population. The U , W components show no systematic variation with M_G as expected. Less obvious features include the deviation in U and W beyond $M_G \approx 15$; this is likely due to contamination by spheroid and thick disk WDs that make up a larger fraction of the population at these magnitudes.

4.2 Velocity dispersion and the local standard of rest

Classically, the main utility of measurements of the mean motion versus velocity dispersion is in estimating the Solar motion with respect to the local standard of rest. This exploits the linear relationship between the velocity dispersion S^2 and rotational lag first identified empirically by Strömberg (1946); the modern theoretical framework for the asymmetric drift relation is described in Binney & Tremaine (2008) (see equation 4.228). In practise this is done by extrapolating the mean velocity to $S^2 = 0$, which provides an estimate of the Solar motion relative to a (hypothetical) population of stars with zero velocity dispersion. Such a population represents newly born stars on closed, circular orbits, the motion of which defines the local standard of rest in the solar neighbourhood.

Figures 5–7 plot the U , V , W components of the mean Solar motion against S^2 along with linear fits. In these plots we have omitted the four points fainter than $M_G = 15.0$ for the reasons outlined in section 4.1. For the U and W components there is no strong correlation and the fit is flat within one sigma, whereas for V

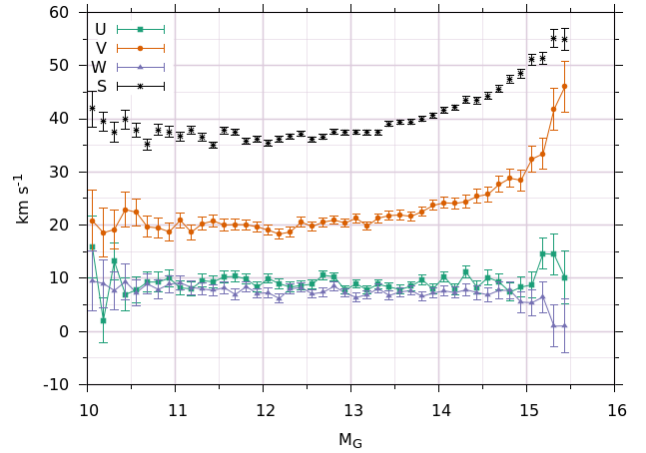


Figure 4. The U , V , W components of the mean Solar motion with respect to the WDs, including a measure of the scalar velocity dispersion S . The trend in V and S is a manifestation of the asymmetric drift arising from the magnitude / age correlation.

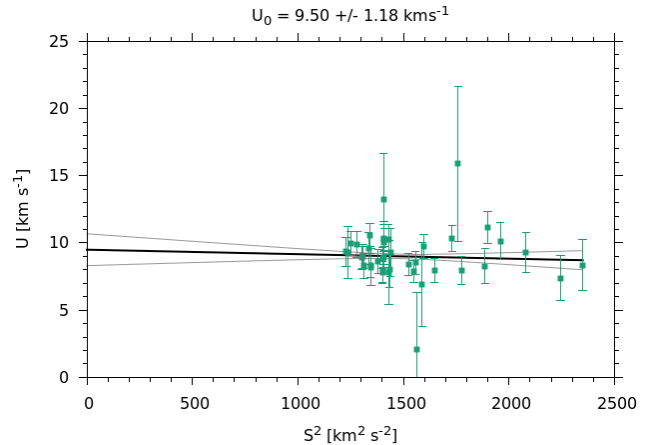


Figure 5. U component of the mean Solar motion versus velocity dispersion; the black line is a linear fit and the grey lines indicate one-sigma confidence intervals.

there is a clear slope. Extrapolating to $S^2 = 0$ yields $(U, V, W)_\odot = (9.50 \pm 1.18, 7.47 \pm 1.21, 8.22 \pm 1.19) \text{ km s}^{-1}$ for the Solar motion with respect to the local standard of rest. Note that relative to similar studies that use MS stars we have few points at low S^2 due to the WDs having a certain minimum age, which results in larger uncertainties due to extrapolating over a longer interval.

4.3 Velocity ellipsoid

In figure 8 we plot the diagonal components of the velocity dispersion tensor against magnitude.¹ In all components the velocity

¹ In this figure and the ones that follow, the plotted quantities are nonlinear functions of our estimated values: the (asymmetric) errorbars depict the 15.87 and 84.13 percentiles of the error distribution, obtained from Monte Carlo integration.

Bin centre M_G [mag]	N [stars]	Mean velocity [kms ⁻¹]			Velocity dispersion [km ² s ⁻²]					
		V_U	V_V	V_W	Σ_{UU}	Σ_{VV}	Σ_{WW}	Σ_{UV}	Σ_{UW}	Σ_{VW}
10.063	82	-15.88	-20.84	-9.49	1846.13	627.04	227.49	562.22	461.50	-207.45
10.188	119	-2.05	-18.56	-9.03	1331.90	685.98	259.71	225.83	-341.21	146.84
10.313	166	-13.20	-19.16	-7.69	1381.77	550.74	140.47	263.70	129.24	321.92
10.438	223	-6.95	-22.92	-9.36	1407.75	626.93	250.58	-1.85	22.80	70.62
10.563	349	-7.81	-22.40	-7.30	1171.79	522.92	417.56	15.16	27.70	82.71
10.688	500	-9.28	-19.68	-8.95	1118.97	471.78	266.60	350.77	73.70	66.07
10.813	635	-9.31	-19.47	-7.89	1248.14	592.03	295.02	165.80	-40.07	18.47
10.938	786	-10.01	-18.75	-8.88	1257.76	498.45	341.81	299.97	-112.53	12.59
11.063	1048	-8.19	-20.91	-9.15	1212.53	550.68	258.01	162.88	72.62	105.13
11.188	1186	-8.00	-18.66	-8.28	1328.73	508.88	308.12	232.68	85.83	116.67
11.313	1390	-9.55	-20.28	-8.00	1199.62	542.13	256.45	193.32	-53.75	-21.61
11.438	1574	-9.34	-20.77	-7.73	1036.90	516.40	281.83	118.39	87.60	-19.37
11.563	1690	-10.25	-20.02	-8.25	1254.47	567.40	314.16	384.97	45.03	-11.15
11.688	2034	-10.35	-20.11	-6.94	1245.43	553.62	313.30	195.89	-0.53	16.19
11.813	2102	-9.89	-20.07	-8.43	1124.08	510.88	301.71	249.59	10.09	31.51
11.938	2243	-8.29	-19.67	-7.14	1196.07	510.06	275.11	162.78	6.94	-19.39
12.063	2224	-9.97	-19.05	-7.28	1158.61	485.98	249.41	244.89	-28.94	17.43
12.188	2371	-8.99	-18.32	-6.20	1177.38	544.20	248.29	266.90	27.85	-7.90
12.313	2500	-8.34	-18.70	-8.00	1197.14	536.58	281.03	231.84	41.84	18.75
12.438	2545	-8.65	-20.56	-8.27	1147.77	581.53	339.41	268.62	25.24	43.65
12.563	2801	-8.89	-19.74	-7.07	1112.51	542.88	302.89	297.00	13.54	-14.77
12.688	2891	-10.58	-20.55	-7.38	1151.91	553.23	314.96	257.92	40.65	12.79
12.813	3133	-10.27	-20.95	-8.48	1200.32	564.73	337.15	178.52	44.53	15.18
12.938	3200	-7.81	-20.41	-7.24	1248.96	533.83	302.04	198.85	16.37	75.86
13.063	3287	-8.95	-21.30	-6.39	1280.43	525.50	278.14	287.91	12.13	37.62
13.188	3319	-7.85	-19.86	-6.91	1246.33	536.79	307.74	289.40	71.29	36.38
13.313	3221	-8.86	-21.29	-8.07	1229.89	527.36	317.62	291.31	-8.16	63.57
13.438	3326	-8.38	-21.79	-6.77	1315.21	607.53	336.40	206.81	68.29	47.08
13.563	3218	-7.87	-21.90	-7.41	1289.66	645.94	362.45	234.84	70.57	63.60
13.688	3142	-8.52	-21.65	-7.70	1449.37	526.23	344.46	254.54	39.18	44.32
13.813	2953	-9.72	-22.54	-6.61	1411.39	598.96	357.67	192.26	-11.50	84.65
13.938	2865	-7.95	-23.69	-7.20	1472.20	616.75	357.78	255.87	-34.56	51.51
14.063	2675	-10.31	-24.21	-7.64	1520.92	684.45	355.90	315.22	6.13	59.11
14.188	2388	-7.97	-24.07	-7.29	1543.36	653.46	441.34	278.35	-66.81	68.07
14.313	1965	-11.16	-24.42	-7.82	1679.18	653.07	489.92	284.11	196.48	67.31
14.438	1690	-8.29	-25.41	-7.32	1621.61	762.39	404.23	195.83	-55.39	-23.96
14.563	1513	-10.15	-25.80	-6.88	1697.80	715.78	477.75	299.89	-51.76	-58.32
14.688	1351	-9.30	-27.65	-7.72	1849.70	684.15	544.75	150.33	-94.65	-52.84
14.813	1225	-7.39	-28.81	-7.73	2002.02	774.65	569.74	400.71	65.81	147.53
14.938	931	-8.34	-28.43	-5.51	1989.77	795.08	682.89	418.77	-183.88	59.79
15.063	687	-8.77	-32.44	-5.42	2259.52	971.15	656.68	344.83	70.88	157.15
15.188	475	-14.64	-33.43	-6.47	2255.08	823.56	823.38	271.34	61.09	106.76
15.313	300	-14.50	-41.76	-0.98	2439.98	1153.29	935.68	43.40	14.91	-32.18
15.438	188	-10.10	-46.06	-1.03	2078.84	1463.10	998.57	-103.49	545.14	-228.99

Table 1. For each magnitude bin, we present the mean stellar velocity relative to the Sun (columns 3–5) and the velocity dispersion tensor (columns 6–11). Units are kms⁻¹ and km²s⁻² respectively, and quantities are referred to the Galactic coordinate frame with principal axes U (towards Galactic centre), V (in the direction of rotation) and W (towards the north Galactic pole).

dispersion increases towards faint magnitudes, although it seems the rate of increase in the V component is smaller. The velocity dispersion is in general larger than that of MS stars, as the mean age of WDs is larger due to the lack of young, newly formed stars: towards the faintest magnitudes nearly all the WDs are very old.

The velocity dispersion tensor has some significant off-diagonal elements, indicating that the velocity ellipsoid is not aligned with the U, V, W axes of the Galactic frame. This can be quantified by the *vertex deviation* l_{XY} , which is the angle by which one has to rotate the velocity ellipsoid in the XY plane to bring it into alignment. The vertex deviation in each of the UV, UW and VW planes is plotted in figure 9. The deviations in the UW and VW planes, which involve the velocity dispersion in the direction

out of the plane, are consistent with zero, whereas a nonzero deviation of around 15° is observed in the UV plane. These results are similar to those of DB98, who find $l_{UV} \approx 20^\circ$ for early spectral types and $10^\circ \pm 4^\circ$ for old disk stars, although we find that the vertex deviation in UV is roughly constant with no obvious trend with magnitude and, equivalently, mean age. Figures 10–12 present projections of the velocity dispersion tensor into each of the UV, UW and VW planes, which helps to visualise the velocity ellipsoid orientation, scale and evolution with magnitude. Ellipses are drawn at the one-sigma level.

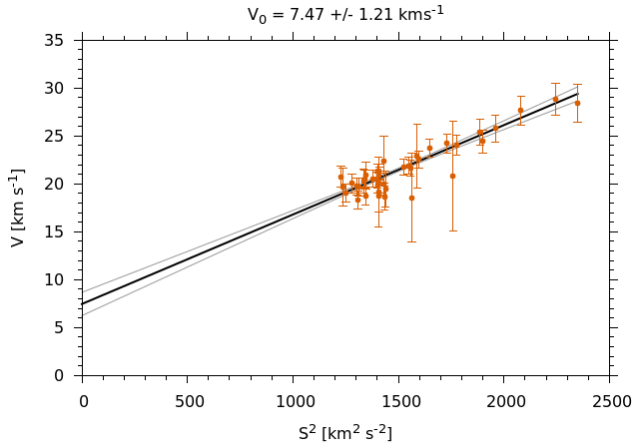


Figure 6. V component of the mean Solar motion versus velocity dispersion.

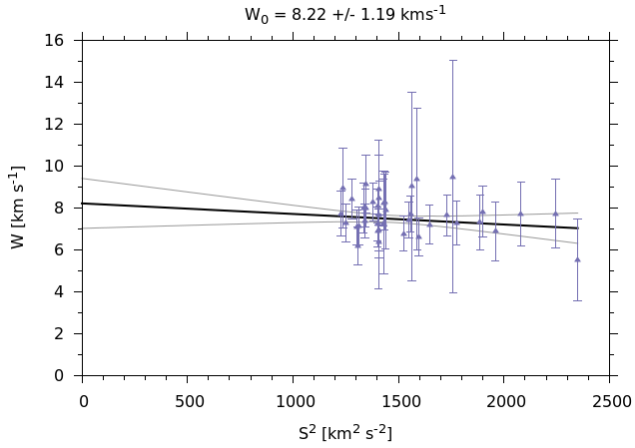


Figure 7. W component of the mean Solar motion versus velocity dispersion.

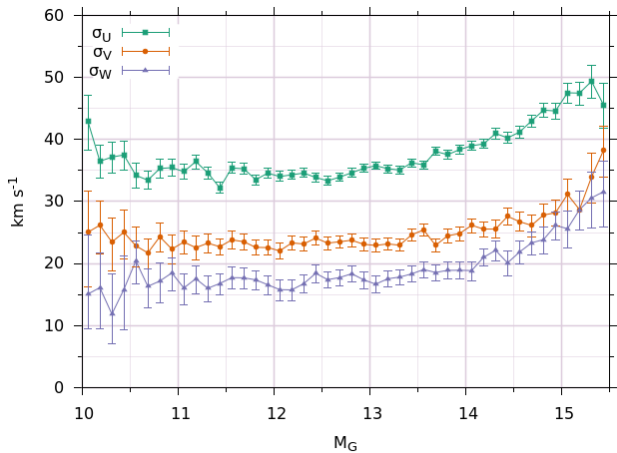


Figure 8. Components of the velocity dispersion tensor along the axes of the Galactic coordinate frame.

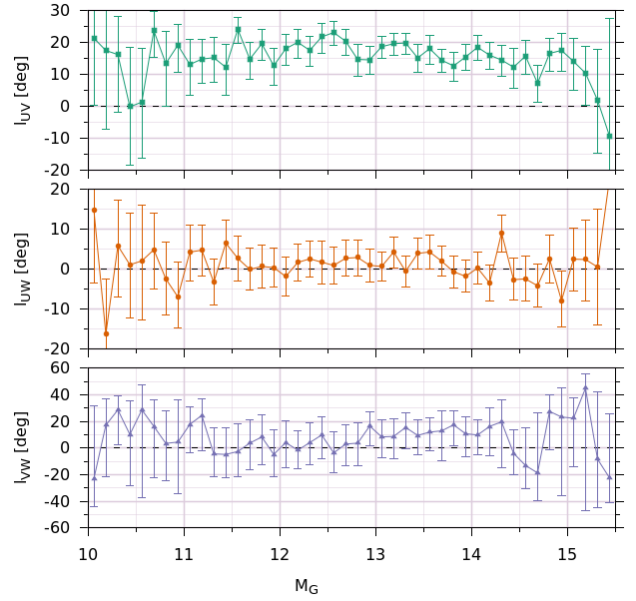


Figure 9. Vertex deviation in each of the UV , UW and VW planes. The deviations in the UW and VW planes, which involves the velocity dispersion in the direction out of the plane, are consistent with zero, whereas a nonzero deviation of around 15 degrees is observed in the UV plane.

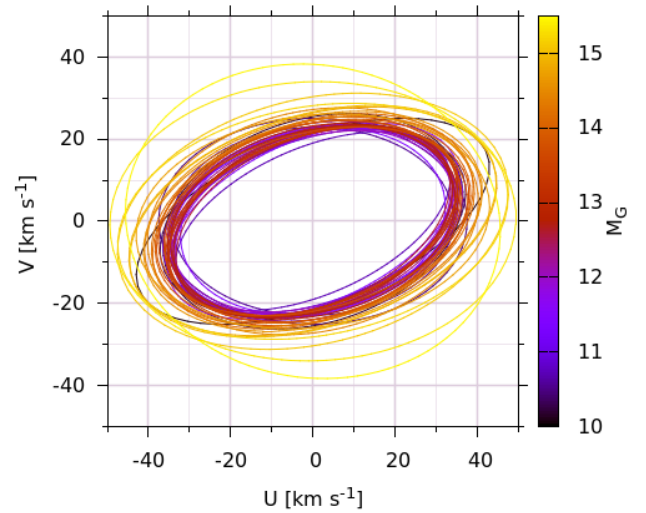


Figure 10. Projection of the velocity ellipsoid onto the UV plane. Ellipses are drawn at the one-sigma level.

5 DISCUSSION

Our values for U_\odot and W_\odot agree within one sigma with the values obtained by both Schönrich et al. (2010) and DB98. However, our value for $V_\odot = 7.47 \pm 1.21$ differs from the Schönrich et al. (2010) value of $V_\odot = 12.24 \pm 0.47$ by $\approx 3.7\sigma$ and from the Kawata et al. (2019) value of $V_\odot = 12.4 \pm 0.7$ by a similar amount, be-

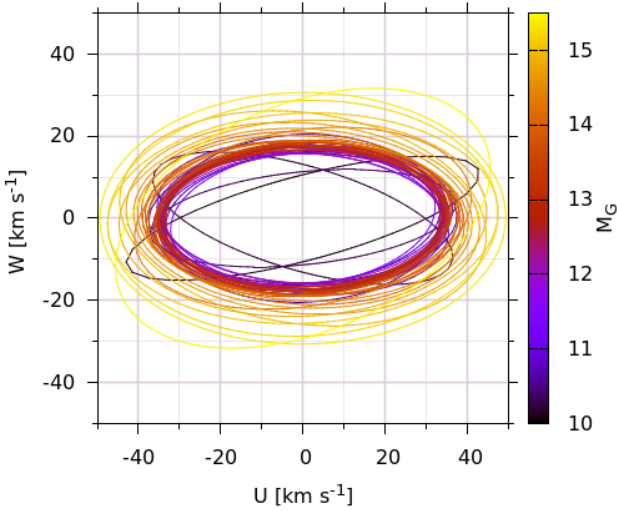


Figure 11. Projection of the velocity ellipsoid onto the UW plane, as per figure 10

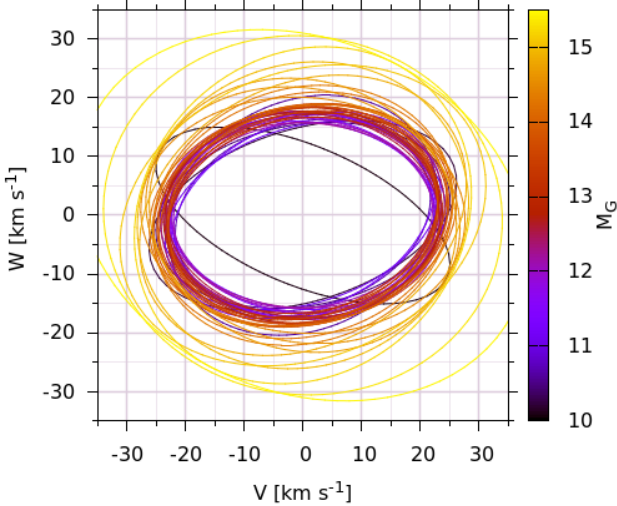


Figure 12. Projection of the velocity ellipsoid onto the VW plane, as per figure 10

ing more in line with the value of $V_{\odot} = 5.25 \pm 0.62$ obtained by DB98. As explained in Schönrich et al. (2010) the DB98 value for V_{\odot} is affected by systematics arising from the metallicity gradient in the disc; briefly, metal-rich stars generally formed at $R < R_0$ and visit the Solar neighbourhood close to the apocentre of their orbit where their azimuthal velocities lag behind the local circular speed. Increasing metallicity shifts the MS to the right in the colour-magnitude plane, introducing a velocity gradient across the

MS and biasing the color/age correlation. The fact that our value of V_{\odot} lies between the DB98 and Schönrich et al. (2010) value could indicate that our WD sample is affected to a lesser extent by similar systematics. Although the location of a WD in the colour-magnitude diagram is independent of the progenitor metallicity to first order, in a population of stars the metallicity-dependent progenitor lifetimes could play a role in introducing kinematic substructures in the WD colour-magnitude plane similar to those described by Schönrich et al. (2010). In addition, over the magnitude range of interest to this study the Gaia WD sequence splits into two branches, due mostly to atmospheric composition but also to the presence of massive WDs possibly formed through stellar mergers (Kilic et al. 2018; El-Badry et al. 2018). The question of to what extent this affects the kinematics as a function of M_G is complex. The WD cooling rate depends on both atmosphere composition and mass, so both of these properties will affect the age distribution of stars as a function of M_G . While the kinematics are likely to be independent of atmosphere type (DA / non-DA), massive WDs formed from merged binary systems could conceivably have different kinematics. Ultimately, both of these effects could lead to kinematic substructure in the WD colour-magnitude diagram and be responsible for systematic errors in our results. However, a thorough investigation of this is outwith the scope of our study. It is also possible that large scale streaming motions within the disk are affecting our results, due to the local nature of our sample. For example, Bovy et al. (2015) finds that the Solar neighbourhood is likely affected by a streaming motion of the order of 10 km s^{-1} in the direction of rotation, which would bias our estimate of V_{\odot} .

The nonzero vertex deviation in the UV plane is understood to be caused by the non-axisymmetric Galactic potential in the disc, likely due to the effect of the spiral arms. The fact that the vertex deviation is independent of magnitude indicates that this has been stable for a long period. No such asymmetry in the potential in the UW and VW planes is evident.

Previous WD proper motion surveys and luminosity function studies that used RPM selection generally assume a constant value for the reflex Solar motion and WD velocity distribution when computing correction factors for stars that fall below the $v_{\text{tan}} \approx 30 \text{ km s}^{-1}$ selection threshold. This includes Harris et al. 2006; RH11; Lam et al. 2019. As shown in this study, there is a strong correlation between WD absolute magnitude and both the mean and dispersion of the heliocentric velocity, which will cause the correction factors to be somewhat overestimated towards the faint end of the luminosity function, leading to an overestimation of the spatial density for faint WDs.

For example, the study of RH11 adopted a mean velocity of $(U, V, W)_{\odot} = (8.62, 20.04, 7.1) \text{ km s}^{-1}$ and velocity dispersion $(\sigma_U, \sigma_V, \sigma_W) = (32.4, 23.0, 18.1) \text{ km s}^{-1}$ with no off-diagonal terms. In conjunction with their lower tangential velocity threshold of 30 km s^{-1} this leads to a sky-averaged discovery fraction of $\approx 57\%$, which is then used to correct the estimated spatial density to account for the missing low velocity stars. However for faint WDs both the mean velocity and velocity dispersion are significantly larger than these values; adopting instead the values that we measure for the M_G bin centred on 14.563 we get a sky-averaged discovery fraction of $\approx 68\%$, meaning that the RH11 study will to first order overestimate the spatial density of WDs of these magnitudes by around a factor ≈ 1.2 , although the true figure depends on the complex effects of the magnitude-dependent proper motion limits when computing the generalised survey volume, as described in Lam et al. (2015).

6 CONCLUSIONS

We have presented the first detailed analysis of the kinematics of Galactic disc WD stars in the Solar neighbourhood, based on a large, kinematically unbiased sample of WDs with absolute astrometry provided by Gaia DR2. Various classical properties of the Solar neighbourhood kinematics have been detected for the first time in the WD population. These are found to be largely consistent with expectations based on MS star studies, although form an independent measure. The results of this study provide an important input to proper motion surveys for white dwarfs, which require knowledge of the velocity distribution in order to correct for missing low velocity stars that are culled from the sample to reduce subdwarf contamination.

ACKNOWLEDGEMENTS

This work has made use of data from the European Space Agency (ESA) mission *Gaia* (<https://www.cosmos.esa.int/gaia>), processed by the *Gaia* Data Processing and Analysis Consortium (DPAC, <https://www.cosmos.esa.int/web/gaia/dpac/consortium>). Funding for the DPAC has been provided by national institutions, in particular the institutions participating in the *Gaia* Multilateral Agreement.

REFERENCES

- Binney J., Tremaine S., 2008, *Galactic Dynamics: Second Edition*. Princeton University Press
- Bovy J., 2017, *MNRAS*, **468**, L63
- Bovy J., Bird J. C., García Pérez A. E., Majewski S. R., Nidever D. L., Zasowski G., 2015, *ApJ*, **800**, 83
- Dehnen W., Binney J. J., 1998, *MNRAS*, **298**, 387
- El-Badry K., Rix H.-W., Weisz D. R., 2018, *ApJ*, **860**, L17
- Feast M., Whitelock P., 1997, *MNRAS*, **291**, 683
- Gaia Collaboration et al., 2016, *A&A*, **595**, A1
- Gaia Collaboration et al., 2018a, *A&A*, **616**, A1
- Gaia Collaboration et al., 2018b, *A&A*, **616**, A11
- Gentile Fusillo N. P., et al., 2018, preprint, ([arXiv:1807.03315](https://arxiv.org/abs/1807.03315))
- Harris H. C., et al., 2006, *AJ*, **131**, 571
- Kawata D., Bovy J., Matsunaga N., Baba J., 2019, *MNRAS*, **482**, 40
- Kepler S. O., et al., 2015, *MNRAS*, **446**, 4078
- Kilic M., et al., 2006, *AJ*, **131**, 582
- Kilic M., Hambly N. C., Bergeron P., Genest-Beaulieu C., Rowell N., 2018, *MNRAS*, **479**, L113
- Kleinman S. J., et al., 2013, *ApJS*, **204**, 5
- Lam M. C., Rowell N., Hambly N. C., 2015, *MNRAS*, **450**, 4098
- Lam M. C., et al., 2019, *MNRAS*, **482**, 715
- Lindgren L., 2018, Re-normalising the astrometric chi-square in Gaia DR2, GAIA-C3-TN-LU-LL-124, http://www.rssd.esa.int/doc_fetch.php?id=3757412
- McMillan P. J., Binney J. J., 2009, *MNRAS*, **400**, L103
- Mestel L., 1952, *MNRAS*, **112**, 583
- Mignard F., 2000, *A&A*, **354**, 522
- Munn J. A., et al., 2017, *AJ*, **153**, 10
- Rowell N., 2013, *MNRAS*, **434**, 1549
- Rowell N., Hambly N. C., 2011, *MNRAS*, **417**, 93
- Schönrich R., Binney J., Dehnen W., 2010, *MNRAS*, **403**, 1829
- Strömberg G., 1946, *ApJ*, **104**, 12
- van Leeuwen F., ed. 2007, *Hipparcos, the New Reduction of the Raw Data* Astrophysics and Space Science Library Vol. 350, doi:10.1007/978-1-4020-6342-8.

APPENDIX A: ADQL QUERY

The ADQL query used to select our initial sample from the Gaia archive is shown below. This returns a table containing 3061480 rows, which is subject to additional filtering as described in section 2.

```
SELECT *
FROM   gaiadr2.gaia_source
WHERE  parallax_over_error > 5.0
      AND phot_bp_mean_flux_over_error > 10
      AND phot_rp_mean_flux_over_error > 10
      AND astrometric_n_good_obs_al > 5
      AND phot_bp_rp_excess_factor BETWEEN
        1.0 + (0.03*POWER(bp_rp, 2.0))
        AND 1.3 + (0.06*POWER(bp_rp, 2.0))
      AND 1000.0/parallax < 250
```

This paper has been typeset from a \LaTeX file prepared by the author.